Available online at www.sciencedirect.com
SCIENCE DIRECT®
International Journal of Heat and Mass Transfer 48 (2005) 75–81
International Journal of HEAT and MASS TRANSFER
www.elsevier.com/locate/ijhmt

Numerical and experimental study on silica generating counterflow diffusion flames

J.I. Kim, J.Y. Hwang [1], J. Lee [1], M. Choi [*,1], S.H. Chung

School of Mechanical and Aerospace Engineering, Seoul National University, Seoul 151-742, Korea

Received 13 December 2003; received in revised form 26 May 2004

Abstract

Temperatures and concentrations of OH radicals in silica generating counterflow oxy-hydrogen diffusion flames are measured using a broadband coherent anti-Stokes Raman spectroscopy (CARS) and a planar laser induced fluorescence (PLIF) techniques to study thermo-chemical effects of $SiCl_4$ addition to flames. Numerical analysis considering detailed chemical reactions including silica generating reactions is also conducted. The experimental results demonstrate that temperatures decrease in preheated zone due to the increase in specific heat of the gas mixture while the decrease is mitigated in particle formation zone due to the heat release through hydrolysis and oxidation reactions of $SiCl_4$. Also, OH concentrations significantly decrease in silica formation flame, which can be attributed to the consumption of oxidative radicals during the silica generating reactions of $SiCl_4$ and depletion of OH by HCl. The numerical simulation agrees well for flames having relatively low flame temperatures of 1750 K but underestimates the decrease in OH concentration for high temperature flame over 2700 K. The disagreement for the high temperature flames would imply possible OH consumption via direct reactions between OH radicals and silicon chlorides, which is expected to be highly sensitive to temperature.

Keywords: Flame synthesis of silica particles; Counterflow diffusion flame; CARS; PLIF

1. Introduction

Flame aerosol synthesis or flame hydrolysis deposition (FHD) using silicon tetrachloride ($SiCl_4$) and oxy-hydrogen flame is one of the most practical and frequently adopted method to produce high quality silica particles or planar waveguides [1,2]. However, understanding of silica formation in a flame is rather limited due to lack of knowledge in chemistry of silicon chlorides and experimental difficulty in the measurement for particle existing flames. Moreover, effect of dopant addition and aerosol formation on a flame has not been systematically investigated even though formation and growth of particles are highly coupled with temperatures and species concentrations in a flame [3].

Although previous analyses on silica formation frequently omitted changes of flame structure caused by dopant addition and particle formation [4], some experimental results have revealed that the effect of dopant addition and aerosol formation on flame structure should not be neglected [5,6]. Recently, Hwang et al.

* Corresponding author. Tel.: +82 2 880 7128; fax: +82 2 878 2465.
E-mail address: mchoi@plaza.snu.ac.kr (M. Choi).
[1] Also at National CRI Center for Nano Particle Control, Institute of Advanced Machinery and Design, Seoul National University, Seoul 151-742, Korea.

0017-9310/$ - see front matter © 2004 Elsevier Ltd. All rights reserved.
doi:10.1016/j.ijheatmasstransfer.2004.06.040

[6] measured temperatures and OH radicals in silica generating coflow diffusion flames using coherent anti-Stokes Raman scattering (CARS) and laser induced fluorescence techniques, respectively. The result was that even small amount of $SiCl_4$ addition could change thermo-chemical structure of a flame significantly. Understanding of interaction between flame and particle growth is important for the controlled formation of nanoparticles in flames [7].

Motivated by this, the present study measures temperatures and concentrations of OH radicals in silica generating counterflow oxy-hydrogen diffusion flames to study thermo-chemical effects of $SiCl_4$ addition to flames. Numerical analysis with detailed chemistry including silica generating reactions from $SiCl_4$ is also conducted to model both flame and particle generation.

2. Experiment and numerical analysis

A counterflow burner consists of a pair of rectangular nozzles having 12.7×63.5 mm cross section and 15.0 mm separation distance whose configuration is shown in Fig. 1 [8]. Either $H_2/N_2/SiCl_4$ mixtures or H_2/N_2 mixtures are supplied through the lower nozzle and O_2/N_2 mixtures are supplied through the upper nozzle, respectively, to form planar oxy-hydrogen diffusion flames with or without particle generation. Two pairs of cases having different flame temperatures are tested to investigate temperature effect on particle generation. In each case, flame characteristics with $SiCl_4$ addition in fuel stream is compared with those without $SiCl_4$. In the low temperature case without particle generation, hydrogen and nitrogen are supplied through the lower fuel nozzle at the flow rate of 1.0 and 3.0 liter per minute (lpm) and oxygen and nitrogen at the flow rate of 0.7 and 3.0 lpm through the upper oxidizer nozzle, respectively. For the high temperature case without particle generation, both hydrogen and nitrogen are supplied through the fuel nozzle at the flow rate of 2.0 lpm and, through the oxidizer nozzle, oxygen and nitrogen at the flow rate of 1.4 and 1.1 lpm, respectively. In case with particle generation, 0.1 lpm of $SiCl_4$ vapor is added to fuel mixture instead of the same amount of nitrogen. The flow conditions for the cases tested are shown in Table 1.

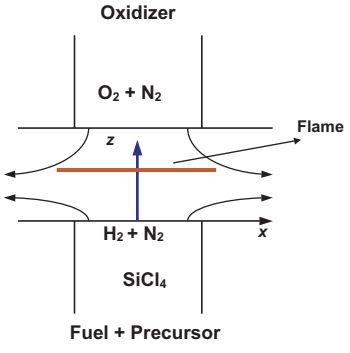

Fig. 1. Schematic of counterflow burner.

The present study adopts a broadband coherent anti-Stokes Raman spectroscopy (CARS) from nitrogen to measure temperature [6], which is appropriate for measuring temperatures in silica generating flames since the signal efficiency is high and the corresponding Raman shift of nitrogen can be effectively isolated from those of other species and silica particles [9,10]. The CARS system adopts a folded box-type optical geometry [11] and corresponding measuring volume has about 25 μm diameter and 0.5 mm length. A Q-switched Nd:YAG laser (Spectra Physics, GCR-150) is used as a pump laser which emits 10 Hz pulsed laser beam with 532 nm wavelength, 7 ns duration, 1 cm^{-1} line width, and 250 mJ energy per pulse. A modeless dye laser emits Stokes beam having 100 cm^{-1} bandwidth, 607 nm mean wavelength, and 15 mJ energy per pulse. Signal detection part consists of a monochromator (Acton, AM510; 1200 gv/mm) and an optical multi-channel analyzer (OMA; Princeton Instruments, IRY-700G/RB), having 1 cm^{-1} resolution. Experimental detail for the CARS measurement is described in Hwang et al. [6].

Concentrations of OH radicals have been measured qualitatively by using a PLIF technique [12]. For the excitation of OH radical, $Q_1(6)$ line of 282.95 nm with $A^2\Sigma^+ - X^2\Pi(1,0)$ transition is adopted since this has been reported to result in the weakest temperature dependence of the fluorescence signal across the flame field of view, [13,14]. An optical system comprising a Nd:YAG laser (Continuum, PL8000), a dye laser (Continuum, ND6000), and a frequency doubler (Continuum, UVT) generates an incident laser sheet beam of 15 mm × 300 μm size having 10 ns duration, 1 cm^{-1} line width, and 10^7 $W/cm^2/cm^{-1}$ spectral intensity which is relatively high compared to saturation intensity for OH excitation [10]. An ICCD camera (Princeton Instrument, ICCD-576) with 576×384 pixels equipped with

Table 1
Flow rates for the tested cases (units in liter per minute at 298 K and 1 bar)

Case	Upper nozzle			Lower nozzle	
	H_2	N_2	$SiCl_4$	O_2	N_2
I	1.0	3.0	0	0.7	3.0
II	1.0	2.9	0.1	0.7	3.0
III	2.0	2.0	0	1.4	1.1
IV	2.0	1.9	0.1	1.4	1.1

WG 305 and UG 11 filters detects fluorescence signals. Light scattering from silica particles has been monitored to visualize silica particles by using 532 nm planar laser sheet beam from the Nd:YAG laser and the ICCD camera as a light source and a detector, respectively.

Numerical calculations were conducted to model silica generation and possible changes in flame structure with the silica generation. Reaction mechanism consists of 19 species and 43 reaction steps including 19 oxy-hydrogen reactions [15] and 19 reactions related to chlorinated species [16] as well as silica formation reactions via oxidation [17] and hydrolysis [18] of $SiCl_4$, as listed in Table 2. Governing equations and numerical schemes have been presented in Lee and Chung [19] and Smooke [20]. The effects of thermal diffusion, viscous dissipation, and thermal radiation were neglected and a uniform flow at the nozzle exit was assumed. Thermodynamic and transport properties are calculated using CHEMKIN II [21] and TRANSPORT PACKAGES [22].

3. Results and discussions

3.1. Effect of $SiCl_4$ addition on flame structure

Fig. 2 shows the measured profiles of temperatures, T, and OH fluorescence signals for the lower flame temperature cases with and without $SiCl_4$ as a function of distance from fuel nozzle, Z. The cases are denoted respectively as case II and case I in Table 1. Scattering signals from silica particles for case II is also shown in Fig. 2. The maximum temperature for case I is about 1750 K at $Z \approx 8$ mm and this is similar to case II. However, closer examination of Fig. 2 shows that, when small amount of $SiCl_4$ is added to flame (case II), temperature decreases slightly in preheated zone of $2 < Z < 6$ compared to the flame without $SiCl_4$ (case I), while, in particle zone of $6 < Z < 8$, the temperature decrease is mitigated having steeper increasing rate so that the maximum temperature of the cases I and II are nearly the same. Also, it can be clearly seen that the OH fluorescence signal decreases significantly with $SiCl_4$ addition.

This result is qualitatively consistent with the previous results for coflow diffusion flames [5,6]. Hwang et al. [6] have measured temperatures in coflow oxy-hydrogen diffusion flames with and without $SiCl_4$ addition and they have shown that temperatures decrease in non-reacting preheated zone while they increase in particle formation zone. The previous work suggested that the temperature decrease in preheated zone and their increase in particle formation zone would be due to the increases in both specific heat and density of the gas mixture in preheated zone and heat release through hydrolysis and oxidation reactions of $SiCl_4$ in particle formation zone, respectively [6]. Hwang et al. [6] have also shown that concentrations of OH radicals decrease in particle formation zones and attributed the OH decrease to the consumption of oxidative radicals during the silica generating reactions of $SiCl_4$ and the depletion of OH by HCl.

In order to study systematically the effect of $SiCl_4$ addition and silica generation on flame structure, numerical analysis has been conducted. The present calculation adopted the detailed chemical mechanism based on oxy-hydrogen reactions of Mass and Warnatz [15]. Reactions for silica formation via oxidation [17] and hydrolysis [18] of $SiCl_4$ is modeled as

$$SiCl_4 + H_2O \Rightarrow SiOCl_2 + \text{products} \quad (1)$$

$$SiCl_4 + O_2 \Rightarrow SiO_2Cl_3 + \text{products} \quad (2)$$

$$SiOCl_2 + H_2O \Rightarrow SiO_2 + \text{products} \quad (3)$$

$$SiO_2Cl_3 \Rightarrow SiO_2 + \text{products} \quad (4)$$

$$SiO_2 = SiO_2(S) \quad (5)$$

where the rate of reactions (3) and (4) for the intermediate species and phase transition of silicon dioxides (5) between gas (SiO_2) and solid ($SiO_2(S)$) are assumed sufficiently fast such that the controlling reactions for the SiO_2 generation are reactions (1) and (2) and the phase transition maintains equilibrium state controlled by temperature. Reactions related to chlorinated species suggested by Ho et al. [16] are also added to the scheme. The kinetic model is given in Table 2. The present model does not include aerosol dynamics for the growth of the silica particles even though the silicon oxides generated from reactions (1)–(5) would not remain as monomers. Further modeling for aerosol dynamics of the silica particles should be a future study.

Calculated temperatures and OH concentrations for cases I and II are compared with the experimental results in Fig. 3, demonstrating that the present model successfully predicts temperatures and OH concentrations for both flames with and without $SiCl_4$. Numerical analysis reveals that the temperature decrease with $SiCl_4$ addition in the preheated zone is mainly due to the increase in specific heat of the gas mixture. On the other hand, the increase of the temperature gradient in the particle formation zone results from the exothermic reactions (1)–(5) where the release of latent heat during phase transition of SiO_2 vapor to particle is most important considering that the temperature of the particle zone is sufficiently small compared to the boiling temperature of SiO_2. Also, sensitivity analysis demonstrated that the decrease of OH concentration is owing to HCl generated during hydrolysis of $SiCl_4$ which depletes OH radicals via

Table 2
Rate constants used to model chemical reactions (units in kJ, mol, K, s, cm)

No.	Reaction	$k = BT^n\exp(-E/RT)$		
		B	n	E
H_2/O_2 reactions				
1	$O_2 + H = OH + O$	2.00E + 14	0.0	70.3
2	$H_2 + O = OH + H$	5.06E + 04	2.7	26.3
3	$H_2 + OH = H_2O + H$	1.00E + 08	1.6	13.8
4	$OH + OH = H_2O + O$	1.50E + 09	1.1	0.4
5	$H + H + M = H_2 + M$	1.80E + 18	−1.0	0.0
6	$H + OH + M = H_2O + M$	2.20E + 22	−2.0	0.0
7	$O + O + M = O_2 + M$	2.90E + 17	−1.0	0.0
8	$H + O_2 + M = HO_2 + M$	2.30E + 18	−0.8	0.0
9	$HO_2 + H = OH + OH$	1.50E + 14	0.0	4.2
10	$HO_2 + H = H_2 + O_2$	2.50E + 13	0.0	2.9
11	$HO_2 + H = H_2O + O$	3.00E + 13	0.0	7.2
12	$HO_2 + O = OH + O_2$	1.80E + 13	0.0	−1.7
13	$HO_2 + OH = H_2O + O_2$	6.00E + 13	0.0	0.0
14	$HO_2 + HO_2 \Rightarrow H_2O_2 + O_2$	2.50E + 11	0.0	−5.2
15	$OH + OH + M = H_2O_2 + M$	3.25E + 22	−2.0	0.0
16	$H_2O_2 + H = H_2 + HO_2$	1.70E + 12	0.0	15.7
17	$H_2O_2 + H = H_2O + OH$	1.00E + 13	0.0	15.0
18	$H_2O_2 + O = OH + HO_2$	2.80E + 13	0.0	26.8
19	$H_2O_2 + OH = H_2O + HO_2$	5.40E + 12	0.0	4.2
Silica generating reactions				
20	$SiCl_4 + H_2O \Rightarrow SiOCl_2 + \text{products}$	1.00E + 12	0.0	121.4
21	$SiCl_4 + O_2 \Rightarrow SiO_2Cl_3 + \text{products}$	3.10E + 19	0.0	400.0
22	$SiOCl_2 + H_2O \Rightarrow SiO_2 + \text{products}$	Fast		
23	$SiO_2Cl_3 \Rightarrow SiO_2 + \text{products}$	Fast		
24	$SiO_2 = SiO_2(S)$	Fast		
Chlorinated species reactions				
25	$H + Cl + M = HCl + M$	5.30E + 21	−2.0	−8.3
26	$Cl + Cl + M = Cl_2 + M$	3.34E + 14	0.0	−7.5
27	$Cl + HO_2 = HCl + O_2$	1.08E + 13	0.0	−1.4
28	$Cl + HO_2 = ClO + OH$	2.47E + 13	0.0	3.7
29	$Cl + H_2O_2 = HCl + HO_2$	6.62E + 12	0.0	8.1
30	$Cl + HOCl = Cl_2 + OH$	1.81E + 12	0.0	1.1
31	$ClO + O = Cl + O_2$	9.70E + 12	0.0	2.1
32	$ClO + H_2 = HOCl + H$	6.03E + 11	0.0	58.8
33	$HOCl = Cl + OH$	1.76E + 20	−3.0	236.3
34	$HOCl = H + ClO$	8.12E + 14	−2.1	390.3
35	$HOCl + H = HCl + OH$	9.55E + 13	0.0	31.8
36	$HOCl + O = OH + ClO$	6.03E + 12	0.0	18.2
37	$HOCl + OH = H_2O + ClO$	1.81E + 12	0.0	4.1
38	$HOCl + Cl = HCl + ClO$	7.28E + 12	0.0	0.4
39	$HCl + H = H_2 + Cl$	1.69E + 13	0.0	17.2
40	$HCl + O = OH + Cl$	5.24E + 12	0.0	26.7
41	$HCl + OH = Cl + H_2O$	2.45E + 12	0.0	4.6
42	$Cl_2 + H = HCl + Cl$	8.59E + 13	0.0	4.9
43	$Cl_2 + O = Cl + ClO$	2.51E + 12	0.0	11.3

$$HCl + OH = Cl + H_2O \quad (6)$$

Flames having extremely high flame temperatures are also investigated both experimentally and numerically in order to verify temperature dependency of the present model. Fig. 4 shows the profiles of measured and calculated temperatures and OH concentrations for cases III and IV. The result demonstrates that these cases have extremely high flame temperature over 2700 K and that the present model underestimates the

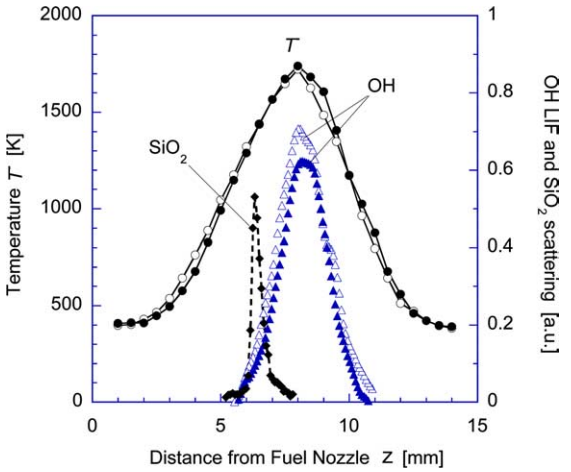

Fig. 2. Distributions of measured temperatures, OH fluorescence signals, and SiO_2 scattering signals for cases I (hollow symbols) and II (solid symbols).

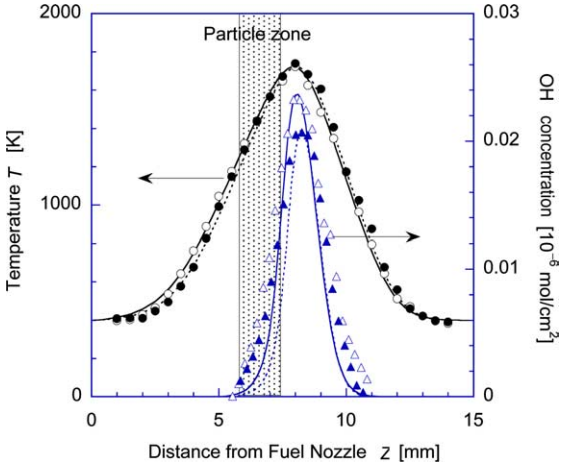

Fig. 3. Measured (symbols) and calculated (lines) profiles of temperatures and OH concentrations. Hollow symbols and solid lines represent case I and solid symbols and dotted lines represent case II, respectively.

decrease in OH concentration with $SiCl_4$ addition. The disagreement for the high temperature flames implies possible OH consumption via direct reactions between OH radicals and silicon chlorides, which is expected to be highly sensitive to temperature.

3.2. Characteristics of silica particle generation

In order to examine the characteristics of silica generation with respect to flame structure, the calculated profiles of temperature, T, particle velocity, U_p, SiO_2 scattering signal, Q_{VV}, and the formation rate of

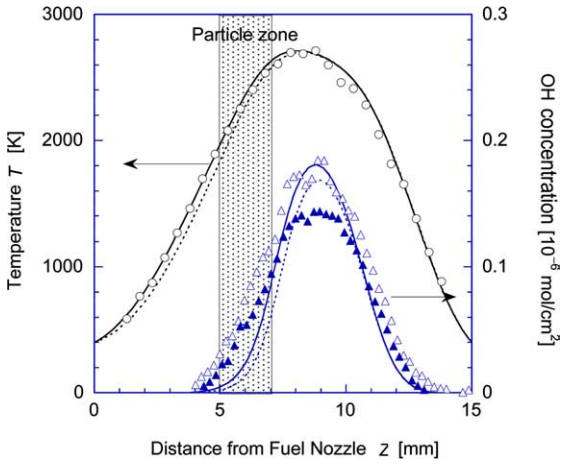

Fig. 4. Measured (symbols) and calculated (lines) profiles of temperatures and OH concentrations. Hollow symbols and solid lines represent case III and solid symbols and dotted lines represent case IV, respectively.

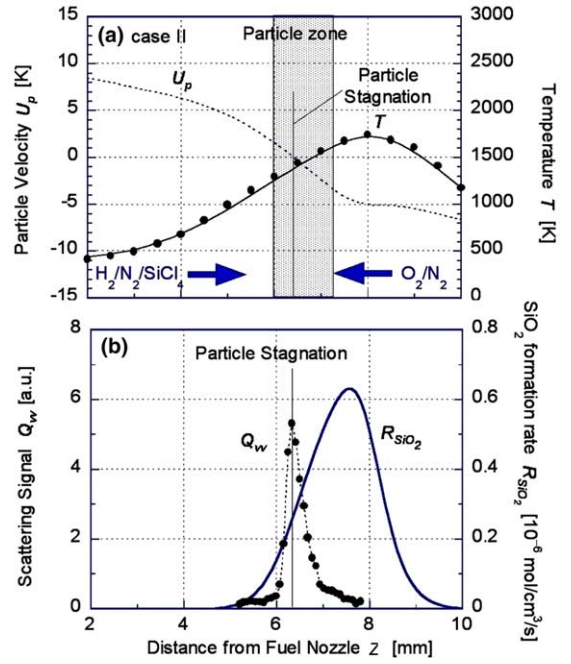

Fig. 5. Distributions of (a) particle velocity and temperature and (b) SiO_2 scattering signal and silica formation rate for case II.

SiO_2(S), R_{SiO_2}, for case II are shown in Fig. 5. Here the particle velocity is determined from gas velocity and thermophoretic velocity assuming the free molecular regime for particles [23,24].

Fig. 5a shows the flame structure of case II. The particle stagnation plane is located at $Z = 6.3$ mm and the

flame is located in the oxidizer side of the stagnation plane near $Z \approx 8$ mm. As shown in Fig. 5b, formation of SiO_2 mainly occurs between the flame and the stagnation plane ($6 < Z < 8.5$ mm) where temperature ranges from 1200 K to 1750 K. Generated SiO_2 monomers coagulate each other moving to stagnation plane so that both the mass concentration and average sizes of the aggregates increase approaching stagnation plane. Therefore, the scattering signal of silica particles show skewed aspects from the flame to the stagnation having maximum value at the particle stagnation plane.

Fig. 6 shows the flame structure and characteristics of particle formation for the high temperature flame (case IV), which are quite different from those of the low temperature flame (case II). Even though the locations of the particle stagnation plane ($Z = 6.4$ mm) and the flame ($Z \approx 8$ mm) are nearly the same with case II, temperatures at the stagnation and flame are over 1000 K higher than those of case II.

More drastic difference appears in characteristics of silica formation. Silica formation occurs in fuel side of the stagnation plane due to elevated temperature in the preheated zone. Consequently, generated particles are transported towards high temperature region undergoing particle growth so that the profile of scattering signal is inversely skewed compared to case II. Moreover, the formation rate has double peaks; the low temperature peak would be attributed to the silica formation by hydrolysis of $SiCl_4$ and the high temperature peak would be resulted from oxidation of $SiCl_4$. Considering that silica formation in this high temperature flame mainly occurs via oxidation close to the flame, the underestimation of OH decrease mentioned above in Fig. 4 might be owing to the consumption of OH radicals during oxidation of silicon chlorides by at high temperature region, which has not been considered in the present modeling.

Interestingly, the scattering signal decreases before the particles reach stagnation plane at $Z = 6.2$ mm where temperature is about 2300 K. This is consistent with the numerical result considering that the calculated silica formation rate decreases rapidly at $Z = 5.9$ and has almost zero at $Z = 6.2$ where the scattering signal starts to decrease. The decrease of scattering signal can be partly responsible to the decrease of scattering cross sections of silica aggregates by sintering process since the rate of sintering process increases fast with temperature. Future studies on aerosol dynamics considering sintering effect are needed to identify the present result for the high temperature flame.

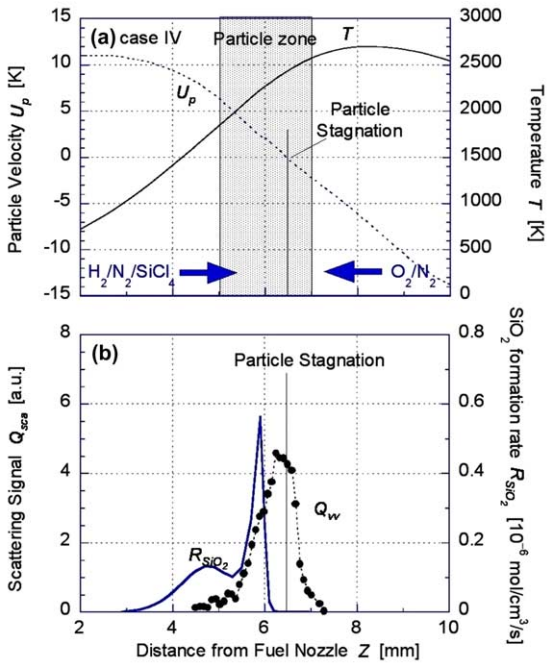

Fig. 6. Distributions of (a) particle velocity and temperature and (b) SiO_2 scattering signal and silica formation rate for case IV.

4. Concluding remarks

Temperatures and concentrations of OH radicals in silica generating counterflow oxy-hydrogen diffusion flames are measured using a broadband CARS and a PLIF techniques to study thermo-chemical effects of $SiCl_4$ addition to flames. Numerical analysis considering detailed chemical reactions including silica generating reactions is also conducted. The experimental results demonstrate that temperatures decrease in preheated zone due to the increase in specific heat of the gas mixture while the decrease is mitigated in particle formation zone due to the heat release through hydrolysis and oxidation reactions of $SiCl_4$. Also, OH concentrations significantly decrease in silica formation flame, which can be attributed to the consumption of oxidative radicals during the silica generating reactions of $SiCl_4$ and the depletion of OH by HCl. The numerical simulation agrees well for flames having relatively low flame temperatures of 1750 K but underestimates the decrease in OH concentration for high temperature flame over 2700 K. The disagreement for the high temperature flames would imply possible OH consumption via direct reactions between OH radicals and silicon chlorides, which is expected to be highly sensitive to temperature.

Acknowledgment

This work was supported by the Creative Research Initiatives from the Korean Ministry of Science and Technology (Center for Nano Particle Control).

References

[1] D. Lee, M. Choi, Control of size and morphology of nanoparticles using CO_2 laser during flame synthesis, J. Aerosol Sci. 31 (10) (2000) 1145–1163.

[2] D. Lee, M. Choi, Coalescence enhanced synthesis of nanoparticles to control size, morphology and crystalline phase at high concentrations, J. Aerosol Sci. 33 (1) (2002) 1–16.

[3] J. Cho, M. Choi, Determination of number density, size and morphology of aggregates in coflow diffusion flames using light scattering and local sampling, J. Aerosol Sci. 31 (2000) 1077–1095.

[4] H.C. Tsai, R. Greif, S. Joh, A study of thermophoretic transport in a reacting flow with application to external chemical vapor deposition processes, Int. J. Heat Mass Tran. 38 (1995) 1901–1910.

[5] M.D. Allendorf, J.R. Bautista, E. Potkay, Temperature measurements in a vapor axial deposition flame by spontaneous Raman spectroscopy, J. Appl. Phys. 66 (1989) 5046–5051.

[6] J.Y. Hwang, Y.S. Gil, J.I. Kim, M. Choi, S.H. Chung, Measurements of temperature and OH radical distributions in a silica generating flame using CARS and PLIF, J. Aerosol Sci. 32 (2001) 601–613.

[7] D. Lee, S. Yang, M. Choi, Controlled formation of nanoparticles utilizing laser irradiation in a flame and their characteristics, Appl. Phys. Lett. 79 (15) (2001) 2459–2461.

[8] C.-H. Hung, J.L. Katz, Formation of mixed oxide powders in flames: Part I. TiO_2–SiO_2, J. Mater. Res. 7 (7) (1992) 1861–1869.

[9] R.H. Stolen, G.E. Walrafen, Water and its relation to broken bond defects in fused silica, J. Chem. Phys. 64 (1976) 2623–2631.

[10] A.C. Eckbreth, Laser Diagnostics for Combustion Temperature and Species, Abacus Press, Tunbridge Well, UK, 1988.

[11] A.C. Eckbreth, G.M. Dobbs, J.H. Stufflebeam, P.A. Tellex, CARS temperature and species measurements in augmented jet engine exhausts, Appl. Opt. 23 (1984) 1328–1339.

[12] M. Alden, H. Edner, G. Hdmstedt, S. Svanberg, T. Hoegberg, Single-pulse laser-induced OH fluorescence in an atmospheric flame, spatially resolved with a diode array detector, Appl. Opt. 21 (1982) 1236–1240.

[13] G. Kychakoff, R.D. Howe, R.K. Hason, Quantitative flow visualization technique for measurements in combustion gases, Appl. Opt. 23 (1984) 704–712.

[14] M.G. Allen, R.K. Hanson, Digital imaging of species concentration fields in spray flames, in: 21st Symposium (International) on Combustion, 1986, pp. 1755–1762.

[15] U. Mass, J. Warnatz, Ignition processes in hydrogen-oxygen mixtures, Combust. Flame 74 (1988) 53–69.

[16] W. Ho, Q.-R. Yu, J.W. Bozzelli, Kinetic study on pyrolysis and oxidation of CH_3Cl in $Ar/H_2/O_2$ mixtures, Combust. Sci. Technol. 85 (1992) 23–63.

[17] D.R. Powers, Kinetics of $SiCl_4$ oxidation, J. Am. Ceram. Soc. 61 (1978) 295–297.

[18] V.F. Kochubei, Kinetics of gas-phase hydrolysis of silicon tetrachloride, Kinet. Catal. 38 (1997) 212–214.

[19] S.D. Lee, S.H. Chung, On the structure and extinction of interacting lean methane/air premixed flames, Combust. Flame 98 (1994) 80–92.

[20] M.D. Smooke, Solution of burner stabilized premixed laminar flames by boundary value methods, J. Comput. Phys. 48 (1982) 72–105.

[21] R.J. Kee, F.M. Ruply, J.A. Miller, Sandia National Laboratories Report, No. SAND 89-8009, 1989.

[22] R.J. Kee, J. Warnatz, J.A. Miller, Sandia National Laboratories Report, No. SAND 83-8209, 1983.

[23] H. Wang, D.X. Du, C.J. Sung, C.K. Law, in: 26th Symposium (International) on Combustion, 1996, pp. 2359–2368.

[24] K.T. Kang, J.Y. Hwang, S.H. Chung, W. Lee, Combust. Flame 109 (1997) 266–281.